IEEE Access
Multidisciplinary | Rapid Review | Open Access Journal

Received March 28, 2022, accepted April 14, 2022, date of publication April 18, 2022, date of current version April 26, 2022.

Digital Object Identifier 10.1109/ACCESS.2022.3168074

Highly-Miniaturized Dual-Mode Bandpass Filter Based on Quarter-Mode Substrate Integrated Waveguide With Wide Stopband

RUSAN KUMAR BARIK[1], (Member, IEEE), SLAWOMIR KOZIEL[1,2], (Fellow, IEEE), AND STANISLAW SZCZEPANSKI[2]

[1]Department of Engineering, Reykjavik University, 102 Reykjavik, Iceland
[2]Faculty of Electronics, Telecommunications and Informatics, Gdańsk University of Technology, 80-233 Gdańsk, Poland

Corresponding author: Slawomir Koziel (koziel@ru.is)

This work was supported in part by the Icelandic Centre for Research (RANNIS) under Grant 217771, and in part by the National Science Centre of Poland under Grant 2018/31/B/ST7/02369.

ABSTRACT This paper presents a novel design of a highly-miniaturized dual-mode bandpass filter (BPF) employing a quarter-mode substrate integrated waveguide (QMSIW). The QMSIW resonator is based on a square cavity with metallic vias along two sides, and open-ended edges at the remaining sides that contain orthogonal feed lines. An open slot is introduced along the two sides of the square cavity with metallic vias to form a magnetic wall. A single metallic via is assigned at the corner of the two open-edged sides to form an electrical wall, which produces different resonances. By loading a slot diagonally, the mode frequencies can be controlled independently, which allows us to realize a second-order BPF. The detailed design steps and a flowchart explaining the filter's topology evolution are presented. The eigen-mode analysis, field distributions, coupling matrix, and full-wave simulation of the proposed QMSIW filter topology are used to determine the filter's operating principle. To verify the proposed theory, a second-order BPF is realized, fabricated, and demonstrated experimentally. The BPF prototype exhibits excellent performance such as a small footprint of $0.019\lambda^2$, a wide passband of 34.8-percent, low insertion loss of 0.43 dB, and a wide stopband of $3.36f_0$ with a rejection level greater than 20 dB. Excellent consistency is found between the EM-simulated and measured responses of the device.

INDEX TERMS Substrate integrated waveguide, quarter-mode, bandpass filter, dual-mode, stopband.

I. INTRODUCTION

Reduced-size high-performance bandpass filters (BPFs) with transmission zeros are critical in the development of modern wireless systems. Due to their advantageous features such as high quality factor, low loss, easy integration, and low cost, substrate integrated waveguides (SIWs) have attracted considerable attention in the recent years [1]–[2]. The SIW technology has been successfully applied to realize various BPFs [3]–[25]. A miniaturized BPF based on the SIW loaded with complementary split-ring resonators (CSRRs) has been designed in [3]. In [4], a three-pole BPF filter has been devised using a SIW triplet structure with frequency dependent cross-coupling. A wideband BPF using U-slotted SIW cavities has been designed in [5]. In [6], a three-pole BPF with controlled transmission zeros has been designed using a dual-mode circular SIW cavity. It has been found that bandpass filters based on full-mode SIW, therefore occupying larger areas, are not suitable for modern compact wireless systems. In order to reduce the size, half-mode SIW cavities are employed, whereas further size miniaturization can be achieved by applying quarter-mode SIW (QMSIW) cavities [7]–[15]. Especially, at low operating frequencies, the QMSIW could be a valuable solution for size-reduced filters of high performance.

Quarter-mode SIW cavities have been illustrated for the development of higher-order bandpass filters in [7]. In [8], half-mode SIW and co-planar waveguide (CPW) resonators

The associate editor coordinating the review of this manuscript and approving it for publication was Dušan Grujić.

have been combined to realize an extended-doublet topology. In [9], multi-layer full-mode SIW square resonators have been employed to design a filter. In [10], a multi-layer dual-mode SIW has been used for the realization of the balanced filter. In [11], a bandpass filter has been designed based on a dual-mode SIW cavity with capacitive patches etched on the top conductor. In [12], a half-mode SIW (HMSIW) rectangular resonator with dual-mode characteristics has been employed for the development of a dual-band filter. A half-mode SIW cavity has been applied to design a dual-mode bandpass filter with two poles and two zeros [13]. In [14], dual-mode bandpass filters have been implemented based on full-mode SIW rectangular cavities. In [15], dual-mode SIW filters with in-line ports have been realized featuring flexible responses. In [16], a third-order SIW lossy filter has been proposed based on complex coupling. In [17], two dual-mode, and one standard SIW cavities have been applied to design a five-pole filter. In [18], a hybrid topology has been developed using a dual-mode SIW and two CPWs to realize fourth-order BPFs. In [19], a triple-order BPF has been proposed by employing the eighth-mode SIW (EMSIW), and the QMSIW cavity. In [20], multi-layered dual-mode SIW with orthogonal feeding has been applied to design a wideband BPF. In [21], a miniaturized BPF with a wide stopband response has been developed using a mix of QMSIW and EMSIW cavities. In [22], multi-layered SIW cavities have been employed to construct a BPF with a large upper stopband response. A wide stopband SIW filter has been obtained using a modified mode suppression approach in [23]. The use of dual-mode SIW rectangular cavities to create box-like BPFs with wide stopband response has been proposed in [24]. The combination of microstrip technology and SIW cavity has been used to build a compact BPF with a wide stopband response in [25]. Although size miniaturization has been achieved by using HMSIW/QMSIW, further and significant size reduction may be possible while retaining a high overall performance, based on the QMSIW cavity.

In this paper, a novel miniaturized second-order bandpass filter with low loss and wide stopband using QMSIW square cavity is proposed. A dual-mode resonance is realized by introducing a ring slot along the metallic vias, and a diagonal ring slot, which enables the design of a second-order Chebyshev filter. The eigen-mode analysis, coupling matrix, and electromagnetic simulation of the presented circuit are provided. The filter features compact size, low insertion loss, wide bandpass, and broad stopband rejection. In addition, two transmission zeros are realized by means of the diagonal ring slot, and a single metallic via. For the sake of demonstration, a compact size second-order BPF with wide bandpass, and low insertion loss is fabricated and experimentally validated.

II. DESIGN PROCEDURE

Figure 1 shows the proposed second-order filter topology, which consists of a square cavity, an open slot, a single metallic via, and a diagonally slot. A step-by-step design evolution of the filter topology has been shown in Fig. 2. First, a full-mode SIW (FMSIW) cavity operating at TE_{110} mode is designed. The FMSIW is then divided into four-sections, each called a quarter-mode SIW (QMSIW). Second, two orthogonal microstrip lines are used for feeding the QMSIW cavity. Subsequently, an open slot is introduced on the top of the QMSIW cavity to form a magnetic wall (MW). Next, a single metallic via is placed at the corner of the two open-edged sides to form an electric wall (EW). The open slot and the single metallic vias produce different mode resonances. Finally, a slot is inserted diagonally on the top of the QMSIW cavity to control the mode resonance frequencies, which allows for synthesizing a second-order BPF. Additionally, the electromagnetic leakage is prevented by the use of the ring slot and a single metallic via. The resonant frequency of the proposed QMSIW can be expressed as [2]

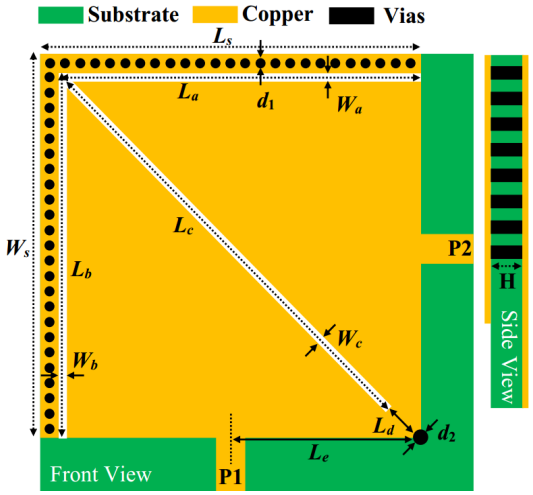

FIGURE 1. Schematic of the QMSIW dual-mode bandpass filter. The optimized dimensions are: $L_s = 30$, $W_s = 30$, $L_a = 28.6$, $W_a = 0.55$, $L_b = 28.6$, $W_b = 0.55$, $L_c = 37$, $W_c = 0.65$, $L_d = 2.6$, $L_e = 14.3$, $d_1 = 0.7$, $d_2 = 1.4$, $H = 0.8$. All units are mm.

$$f_{mn0}^{QMSIW} = \frac{1}{2\pi\sqrt{\varepsilon_r}}\sqrt{\left(\frac{m\pi}{2W_{eq}^{QMSIW}}\right)^2 + \left(\frac{n\pi}{2L_{eq}^{QMSIW}}\right)^2} \quad (1)$$

where

$$\begin{cases} W_{eq}^{QMSIW} = W_s - 1.08\dfrac{d^2}{p} + 0.1\dfrac{d^2}{W_s} \\ L_{eq}^{QMSIW} = L_s - 1.08\dfrac{d^2}{p} + 0.1\dfrac{d^2}{L_s} \end{cases} \quad (2)$$

In order to reduce the leakage loss, the diameter d_1 and the distance S between the vias are chosen based on the conditions $d_1/\lambda \leq 0.1$ and $d_1/S \geq 0.5$ [2]. The eigen-mode solver is used to illustrate the different resonance modes. Figure 3 shows the E-field distributions of the QMSIW cavity without perturbation for different modes (TE_{110}, TE_{210}, and TE_{120}). It can be noted that the maximum field strength is

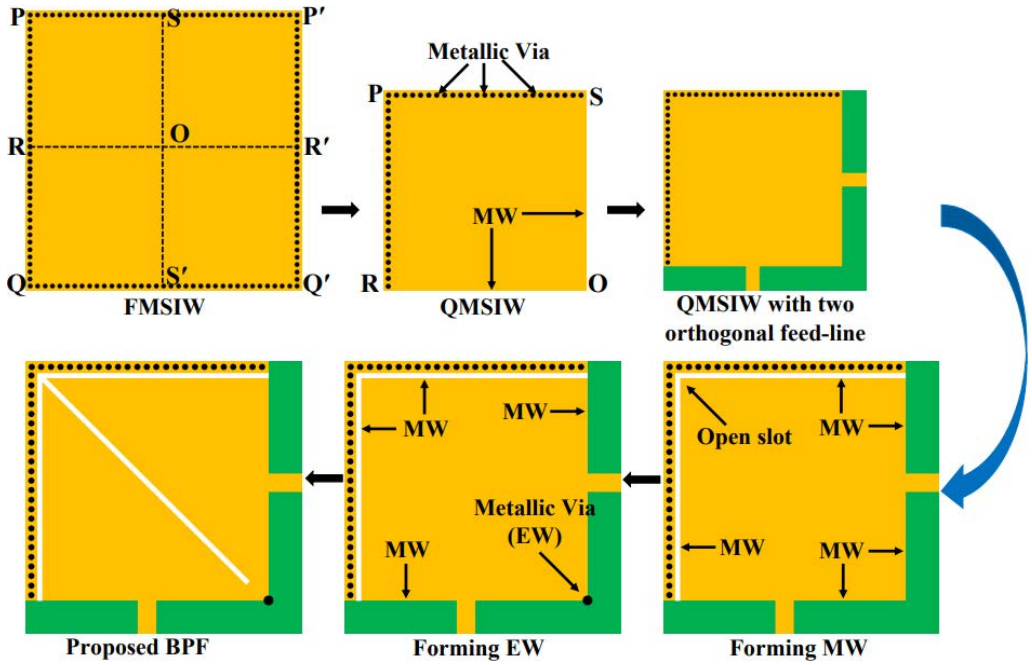

FIGURE 2. Design steps of a highly compact QMSIW BPF.

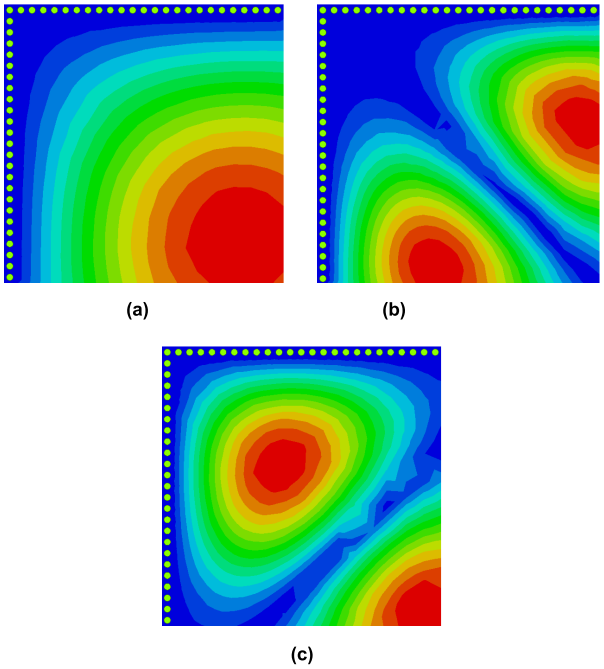

FIGURE 3. E-field distributions of the QMSIW cavity without perturbation for different modes: (a) TE_{110} mode, (b) TE_{210} mode, (c) TE_{120} mode.

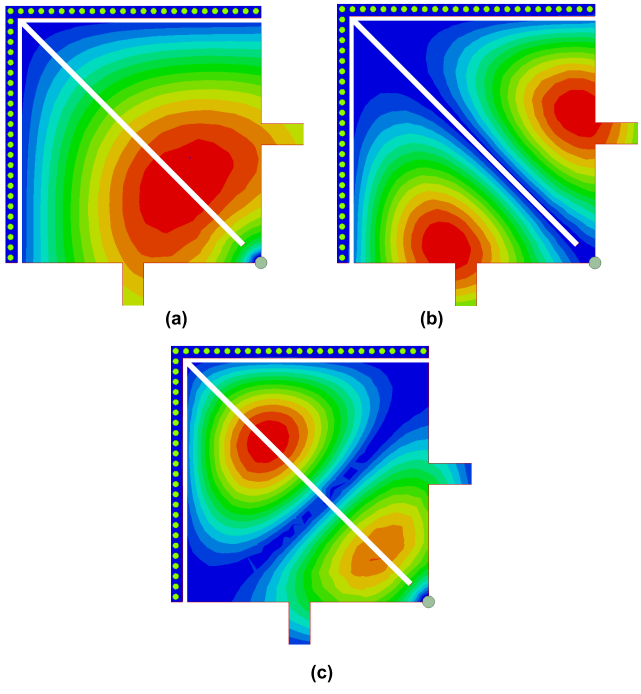

FIGURE 4. E-field distributions of the proposed QMSIW filter for different modes: (a) TE_{110} mode, (b) TE_{210} mode, (c) TE_{120} mode.

observed at the center, the middle of the open-edge sides, and a diagonal position for the TE_{110} mode, TE_{210} mode, and the TE_{120} mode, respectively..

Figure 4 shows the E-field distribution of the proposed QMSIW filter for different modes (TE_{110}, TE_{210}, and TE_{120}), which are obtained by employing the eigen-mode solver. It is observed that the E-field distributions of the proposed QMSIW filter for TE_{110} and TE_{120} modes are different from the TE_{110} and TE_{120} modes of the QMSIW cavity without perturbation as shown in Figs. 3(a) and (c), respectively. On the other hand, the proposed QMSIW filter barely changes the E-field distribution for TE_{210} mode due to the diagonal

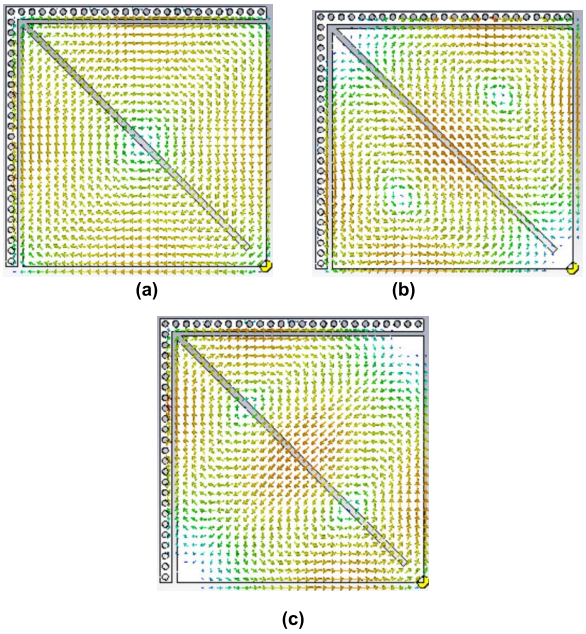

FIGURE 5. Surface current distributions for different modes: (a) TE_{110} mode, (b) TE_{210} mode, (c) TE_{120} mode.

slot, which is placed at the null electric field of this mode as depicted in Fig 4(b).

Figure 5 shows the surface current distribution for the three resonant modes (TE_{110}, TE_{210}, and TE_{120}). By introducing a diagonal ring slot, the resonant mode frequencies can be controlled independently. To demonstrate the influence of the slot, the variation of mode frequencies as a function of the slot length L_c has been depicted in Fig. 6. Referring to Figs. 5(a) and 5(c), the surface current distributions for TE_{110} and TE_{120} modes are perpendicular to the diagonal ring slot, which results in a reduction of the resonant frequencies. From Fig. 5(b), it can be observed that the surface current distribution for TE_{210} mode is parallel to the diagonal ring slot so that the ring has little influence on the TE_{210} mode frequency. The resonant frequencies for the TE_{110} and TE_{120} modes are decreased by increasing the length of the diagonal ring slot, whereas a flat line is seen for the TE_{210} mode. This feature helps to realize a second-order BPF by bringing the TE_{110} and TE_{120} modes closer, while shifting the TE_{210} mode higher in frequency to achieve a wide stopband response.

The required source and load external quality factors Q_S and Q_L, and the coupling coefficient $K_{i,i+1}$ can be extracted as follows [27]

$$Q_S = Q_L = \frac{\omega_0}{\Delta\omega_{\pm 3dB}} \tag{3}$$

And

$$K_{i,i+1} = \frac{f_{m2}^2 - f_{m1}^2}{f_{m2}^2 + f_{m1}^2} \tag{4}$$

where ω_0 and $\Delta\omega_{\pm 3dB}$ are the center frequency and the 3dB bandwidth, respectively. f_{m1} and f_{m2} are defined as

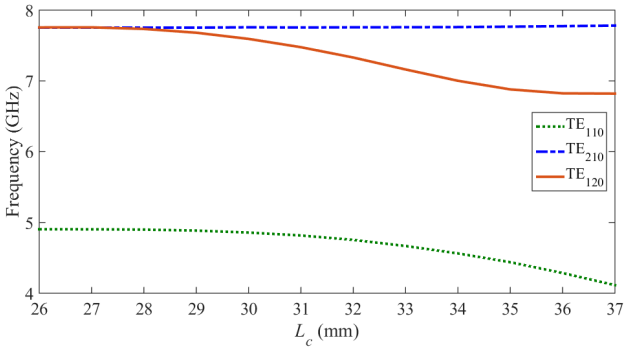

FIGURE 6. Variation of mode frequencies as a function of the length L_c of the diagonal slot.

the mode frequencies. The bandwidth of the filter can be controlled by the length of the diagonal slot. The unloaded quality factor Q_u can be computed by means of the eigen-mode analysis considering the total losses contributed due to the dielectric loss, conductor loss, and radiation loss.

For validation, a second-order Chebyshev filter centered at f_0 of 1.03 GHz with a passband ripple of 0.0218 ($|S_{11}| = -23$ dB) and the fractional bandwidth of 14.6% is designed. According to [27], its lowpass filter parameters are defined as $g_0 = 1$, $g_1 = 0.5521$, $g_2 = 0.4791$, and $g_3 = 1.0735$. The external quality factor, the coupling coefficient, and the coupling matrix are calculated as [27]: $Q_S = Q_L = 7.3$, $K_{12} = 0.0969$ and

$$M = \begin{bmatrix} 0 & 1.3749 & 0 & 0.0224 \\ 1.3749 & 0.5132 & 1.8088 & 0.4106 \\ 0 & 1.8088 & -0.6190 & 1.3121 \\ 0.0224 & 0.4106 & 1.3121 & 0 \end{bmatrix} \tag{5}$$

Q_S, Q_L, and K_{12} are controlled by the length of the diagonal ring slot and the single metallic via. The proposed filter is realized using a quarter-mode cavity to ensure size reduction. The BPF is designed on a 0.8-mm-thick RT/Duroid 5880 substrate ($\varepsilon_r = 2.2$, $\tan\delta = 0.0009$). The unloaded quality factor Q_u of the QMSIW cavity resonator is calculated as 507.6 at the fundamental mode.

The equivalent LC circuit models are generated for the proposed QMSIW filter as shown in Figure 7. The QMSIW cavity is treated as two-wire transmission-lines loaded with metallic vias, which are modelled as shunt inductors L_{v1}. The electric and magnetic couplings at the feed-lines are modelled as C_{c1} and L_{c1}. The QMSIW with the slot resonator is represented as shunt connected LC resonator (L_{sr} and C_{sr}) with their mutual electric and magnetic couplings represented by C_{c2} and L_{c2}. This equivalent circuit is a simplified version, which is validated using the Keysight ADS simulator.

Figure 8 shows the S-parameters obtained from the equivalent circuit model, coupling matrix and EM simulation. An identical response is observed in the passband and the stopband window. Two transmission poles are produced in the passband with a return loss of greater than 23 dB and insertion

TABLE 1. Performance comparison between the proposed design and state-of-the-art SIW filters.

Ref	f_0 (GHz)	FBW (%)	IL (dB)	N	TZs	Upper stopband	Size (λ_g^2)	Techniques
[3]	3.52	6	1.45	4	2	20dB@1.66f_0	0.176	CSRR-loaded SIW
[4]	4.85	3.71	3	3	2	15dB@1.16f_0	2.21	Triplet SIW
[5]	8.5	42	1.1	5	1	20dB@1.45f_0	0.787	U-slotted SIW
[6]	8	3.51	2.15	3	2	20dB@1.25f_0	0.804	Dual-mode SIW
[7]	4	16	1.02	3	1	15dB@1.75f_0	0.0625	QMSIW
[8]	3.7	6.7	1.49	3	2	20@2.65f_0	0.32	HMSIW
[9]	13	4.6	1.7	2	2	20@2.3f_0	0.72	Multi-layered SIW
[10]	15.3	3	2.4	2	2	20@3.27f_0	1.39	Multi-layered SIW
[11]	8	20	0.7	2	2	14dB@1.81f_0	0.176	Dual-mode SIW
[13]	10	5.3	2.4	4	4	30dB@1.05f_0	1.75	HMSIW doublet
[14]	10	3.3	1.55	4	2	30dB@1.03f_0	2	Cascaded doublets
[16]	4.97	20	2.2	3	1	20dB@1.1f_0	NR	Complex coupling
[17]	2.875	7.5	2.91	5	2	20dB@1.66f_0	2.06	Air-filled dual-mode SIW
[18]	5.78	9.47	1.53	4	5	20dB@1.21f_0	0.95	Dual-mode SIW+CPW
[19]	9.1	22	0.9	3	3	NR	0.05	Eighth-mode SIW
[20]	10	3.28	1.15	4	4	20dB@1.1f_0	0.739	Dual-mode SIW
[21]	8	11	0.9	3	3	23dB@0.865f_0	0.147	Quarter and eighth mode cavities
[22]	5	6.6	0.9	3	NR	30dB@4.2f_0	NR	Post-loaded SIW
[23]	7.55	1.84	3.22	3	NR	20dB@3.85f_0	1.61	Varied positions for external and internal couplings
[24]	10.01	3.98	1.52	4	1	20dB@1.67f_0	1.978	Single-mode and dual-mode SIW
[25]	10.11	11.7	1.22	4	2	20dB@2.9f_0	0.5	Hybrid
[26]	1.0	12	0.85	2	NR	26dB@4.5f_0	0.0381	Fan-shaped HMSIW
Design I	**1.03**	**34.8**	**0.43**	**2**	**2**	**20dB@3.36f_0**	**0.019**	**QMSIW with slot**

FBW: Fractional bandwidth, IL: Insertion loss, N: Order, TZ: Transmission zeros, f_0: Center frequency, NR: Not reported

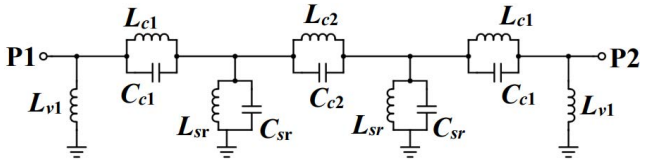

FIGURE 7. Equivalent LC circuit model of the proposed QMSIW filter. The electrical parameters are L_{v1} = 6.813 nH, L_{c1} = 3.896 nH, C_{c1} = 1.09 pF, L_{c2} = 17.324 nH, C_{c2} = 0.343 pF, L_{sr} = 13.455 nH, C_{sr} = 5.068 pF.

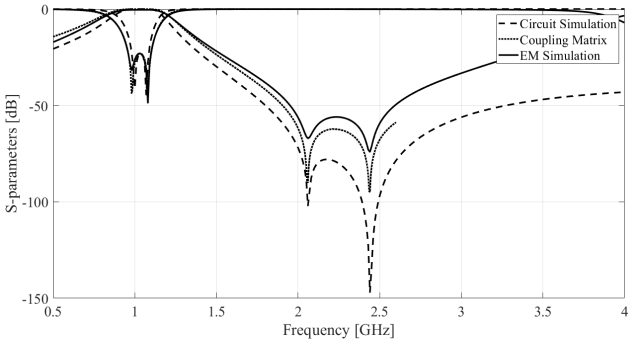

FIGURE 8. Circuit model, coupling matrix, and EM simulated S-parameters.

loss better than 0.41 dB. In addition, two transmission zeros (TZs) are obtained at 2.06 GHz and 2.44 GHz due to the ring slot, and a single metallic via, which enables wide stopband response. It is observed that the transmission zeros can be controlled by the mutual and input couplings at frequencies:

$$f_{TZ1} = \frac{1}{2\pi\sqrt{L_{c1}C_{c1}}} \tag{6}$$

$$f_{TZ2} = \frac{1}{2\pi\sqrt{L_{c2}C_{c2}}} \tag{7}$$

Figure 9 shows the variation of coupling coefficient (K_{12}) versus width (W_c) of the diagonal slot. The EM simulation is used to extract the coupling coefficients in the case of weak couplings in the transmission characteristic. It can be observed that the coupling coefficient decreases with the increase in the slot width. The variation of the external coupling coefficient (Q_e) is determined by varying the parameter L_e as shown in Fig. 10. From the figure, it can be noted that the external coefficient Q_e decreases as L_e increased. Based on the above theoretical investigations,

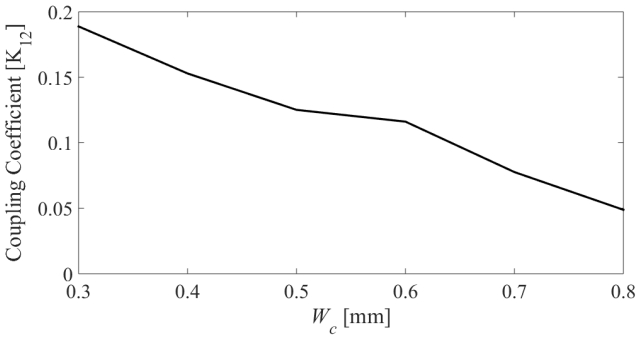

FIGURE 9. Variation of coupling coefficient (K_{12}) with the slot width (W_c).

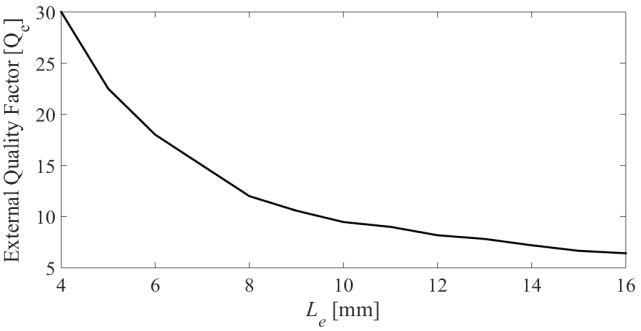

FIGURE 10. Variation of external quality factor (Q_e) by the parameter (L_e).

a detailed synthesis flowchart is provided for the realization of a highly-miniaturized second-order BPF applying QMSIW resonator as shown in Figure 11.

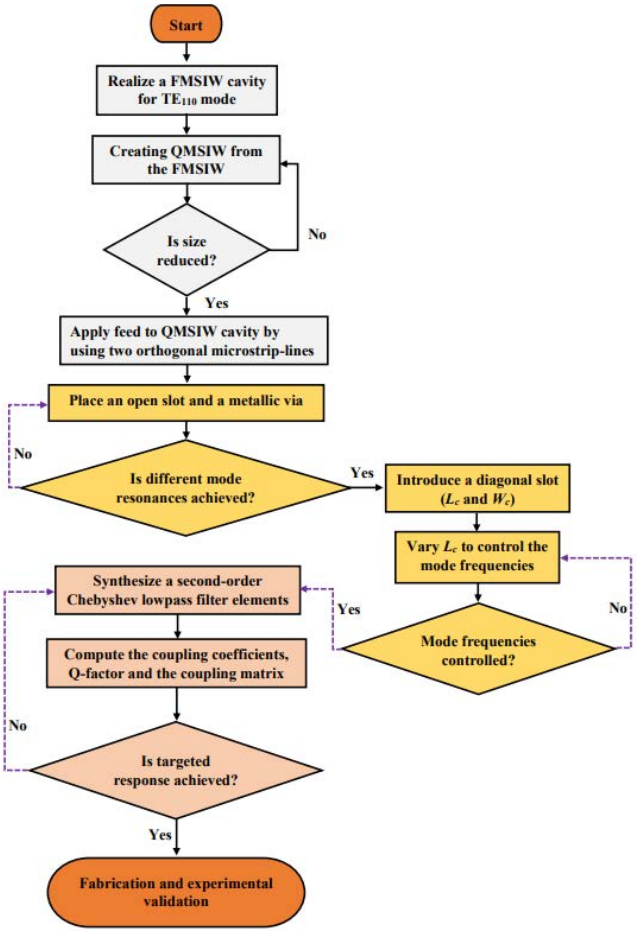

FIGURE 11. Synthesis flowchart of the proposed second-order BPF.

III. FABRICATION, RESULTS AND DISCUSSION

To demonstrate and exemplify the above analysis, a two-pole QMSIW filter operating at 1.03 GHz has been fabricated using the same substrate material as mentioned in Section II. Figure 12 shows the photograph of the second-order filter prototype. The circuit size of the filter prototype is $0.14\lambda \times 0.14\lambda$ ($0.019\lambda^2$). A vector network analyzer (Rohde & Schwarz) is used for the measurement.

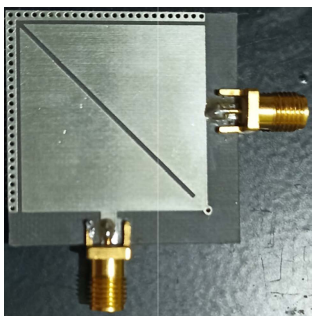

FIGURE 12. Fabricated prototype of the proposed second-order BPF.

Figure 13 shows the EM simulated and measured *S*-parameters of the proposed two-pole QMSIW bandpass filters. The agreement between EM simulation and measurement data is overall excellent. However, a small deviation can be observed due to the connector loss and the fabrication tolerance. The measured operating frequency and the 3-dB fractional-bandwidth are 1.04 GHz and 34.8%, respectively. Two poles are located at 0.98 GHz and 1.08 GHz, respectively. Also, the two transmission zeros are located at 2.06 GHz and 2.44 GHz, respectively. The tested insertion loss and return loss are 0.43 dB and –22.97 dB, respectively. A wide stopband of $3.36f_0$ is obtained with a rejection level better than 20 dB.

Table 1 provides a comparative analysis and benchmarking of the proposed QMSIW filter with respect to the state-of-the-art filter circuits from the literature [3]–[26]. The proposed filter exhibits the footprint area reduced by 49.8% over the smallest of the considered compact circuits (here, [26]). Compared with [3]–[26], the proposed filter achieves lower insertion loss, and a larger fractional bandwidth. Furthermore, the proposed QMSIW filter exhibits a better stopband rejection when compared with [3]–[21] and [23]–[25]. The above analysis indicates that the presented QMSIW BPF can be considered an attractive alternative over the previously reported filters.

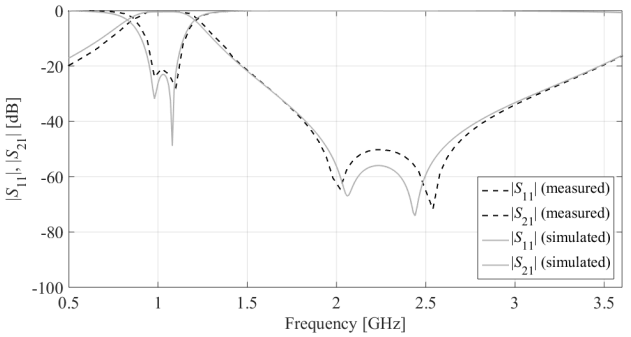

FIGURE 13. EM-simulated and measured performance of the proposed BPF.

IV. CONCLUSION

In this paper, we reported a novel design of a highly miniaturized dual-mode bandpass filter based on the QMSIW square resonator. Magnetic and electric walls are produced by placing an open slot along the metallic vias, and a single metallic via located at the corner of the two open-edged sides, which generates different mode resonances. A ring slot is etched diagonally on the top of the cavity to control the resonant mode frequencies. The working principle of the proposed QMSIW filter has been discussed in detail by using an eigen-mode solution, the coupling matrix, and EM simulation. Finally, a two-pole QMSIW filter with a wide stopband and two zeros has been fabricated and experimentally demonstrated. The circuit size of $0.019\lambda^2$ is highly compact when compared to the state-of-the-art circuits. The measured in-band return loss and insertion loss are –21 dB and 0.43 dB, respectively. The 3-dB bandwidth of 34.8% and a wide stopband of $3.36f_0$ with a rejection level better than 20 dB. Satisfactory agreement between the measured and EM simulated responses corroborates the validity of the presented design approach.

REFERENCES

[1] D. Deslandes and K. Wu, "Single-substrate integration technique of planar circuits and waveguide filters," *IEEE Trans. Microw. Theory Techn.*, vol. 51, no. 2, pp. 593–596, Feb. 2003.

[2] M. Bozzi, A. Georgiadis, and K. Wu, "Review of substrate-integrated waveguide circuits and antennas," *IET Microw., Antennas Propag.*, vol. 5, no. 8, pp. 909–920, Jun. 2011.

[3] Q.-L. Zhang, W.-Y. Yin, S. He, and L.-S. Wu, "Compact substrate integrated waveguide (SIW) bandpass filter with complementary split-ring resonators (CSRRs)," *IEEE Microw. Wireless Compon. Lett.*, vol. 20, no. 8, pp. 426–428, Aug. 2010.

[4] L. Szydlowski, A. Jedrzejewski, and M. Mrozowski, "A trisection filter design with negative slope of frequency-dependent crosscoupling implemented in substrate integrated waveguide (SIW)," *IEEE Microw. Wireless Compon. Lett.*, vol. 23, no. 9, pp. 456–458, Sep. 2013.

[5] R. S. Chen, S.-W. Wong, L. Zhu, and Q.-X. Chu, "Wideband bandpass filter using U-slotted substrate integrated waveguide (SIW) cavities," *IEEE Microw. Wireless Compon. Lett.*, vol. 25, no. 1, pp. 1–3, Jan. 2015.

[6] F. Cheng, X. Q. Lin, M. Lancaster, K. Song, and Y. Fan, "A dual-mode substrate integrated waveguide filter with controllable transmission zeros," *IEEE Microw. Wireless Compon. Lett.*, vol. 25, no. 9, pp. 576–578, Sep. 2015.

[7] S. Moscato, C. Tomassoni, M. Bozzi, and L. Perregrini, "Quarter-mode cavity filters in substrate integrated waveguide technology," *IEEE Trans. Microw. Theory Techn.*, vol. 64, no. 8, pp. 2538–2547, Aug. 2016.

[8] W. Shen, "Extended-doublet half-mode substrate integrated waveguide bandpass filter with wide stopband," *IEEE Microw. Wireless Compon. Lett.*, vol. 28, no. 4, pp. 305–307, Apr. 2018.

[9] D. Jia, Q. Feng, Q. Xiang, and K. Wu, "Multilayer substrate integrated waveguide (SIW) filters with higher-order mode suppression," *IEEE Microw. Wireless Compon. Lett.*, vol. 26, no. 9, pp. 678–680, Sep. 2016.

[10] H.-W. Deng, Y.-K. Han, L. Sun, J.-M. Zhu, and S.-B. Xing, "Multilayer dual-mode balanced SIW filter utilizing PEC–PMC characteristic for common-mode suppression," *IEEE Microw. Wireless Compon. Lett.*, vol. 30, no. 9, pp. 865–868, Sep. 2020.

[11] M. Sánchez-Soriano, S. Sirci, J. D. Martínez, and V. E. Boria, "Compact dual-mode substrate integrated waveguide coaxial cavity for bandpass filter design," *IEEE Microw. Wireless Compon. Lett.*, vol. 26, no. 6, pp. 386–388, Jun. 2016.

[12] K. Zhou, C.-X. Zhou, and W. Wu, "Dual-mode characteristics of half-mode SIW rectangular cavity and applications to dual-band filters with widely separated passbands," *IEEE Trans. Microw. Theory Techn.*, vol. 66, no. 11, pp. 4820–4829, Aug. 2018.

[13] F. Zhu, G. Q. Luo, Z. Liao, X. W. Dai, and K. Wu, "Compact dual-mode bandpass filters based on half-mode substrate-integrated waveguide cavities," *IEEE Microw. Wireless Compon. Lett.*, vol. 31, no. 5, pp. 441–444, May 2021.

[14] F. Zhu, G. Q. Luo, B. You, X. H. Zhang, and K. Wu, "Planar dual-mode bandpass filters using perturbed substrate-integrated waveguide rectangular cavities," *IEEE Trans. Microw. Theory Techn.*, vol. 69, no. 6, pp. 3048–3057, Jun. 2021.

[15] P. Chu, W. Hong, M. Tuo, K.-L. Zheng, W.-W. Yang, F. Xu, and K. Wu, "In-line ports dual-mode substrate integrated waveguide filter with flexible responses," *IEEE Microw. Wireless Compon. Lett.*, vol. 28, no. 10, pp. 882–884, Oct. 2018.

[16] L.-F. Qiu, L.-S. Wu, B. Xie, W.-Y. Yin, and J.-F. Mao, "Substrate integrated waveguide filter with flat passband based on complex couplings," *IEEE Microw. Wireless Compon. Lett.*, vol. 28, no. 6, pp. 494–496, Jun. 2018.

[17] C. Tomassoni, L. Silvestri, A. Ghiotto, M. Bozzi, and L. Perregrini, "Substrate-integrated waveguide filters based on dual-mode air-filled resonant cavities," *IEEE Trans. Microw. Theory Techn.*, vol. 66, no. 2, pp. 726–736, Feb. 2018.

[18] Q. Liu, D. Zhou, D. Lv, D. Zhang, and Y. Zhang, "Ultra-compact highly selective quasi-elliptic filters based on combining dual-mode SIW and coplanar waveguides in a single cavity," *IET Microw., Antennas Propag.*, vol. 12, no. 3, pp. 360–366, Feb. 2018.

[19] X. Wang, X.-W. Zhu, Z. Jiang, Z.-C. Hao, Y.-W. Wu, and W. Hong, "Analysis of eighth-mode substrate-integrated waveguide cavity and flexible filter design," *IEEE Trans. Microw. Theory Techn.*, vol. 67, no. 7, pp. 2701–2712, Jul. 2019.

[20] Q. Liu, D. Zhou, D. Lv, D. Zhang, J. Zhang, and Y. Zhang, "Multi-layered dual-mode substrate integrated waveguide bandpass filter with input and output ports located on same substrate layer," *IET Microw., Antennas Propag.*, vol. 13, no. 15, pp. 2641–2648, Dec. 2019.

[21] P. Kim and Y. Jeong, "Compact and wide stopband substrate integrated waveguide bandpass filter using mixed quarter- and one-eighth modes cavities," *IEEE Microw. Wireless Compon. Lett.*, vol. 30, no. 1, pp. 16–19, Jan. 2020.

[22] B. Lee, S. Nam, S.-W. Jeong, and J. Lee, "Post-loaded substrate-integrated waveguide bandpass filter with wide upper stopband and reduced electric field intensity," *IEEE Microw. Wireless Compon. Lett.*, vol. 30, no. 4, pp. 371–374, Apr. 2020.

[23] H.-W. Xie, K. Zhou, C.-X. Zhou, and W. Wu, "Wide-stopband SIW filters using modified multi-spurious modes suppression technique," *IEEE Trans. Circuits Syst. II, Exp. Briefs*, vol. 67, no. 12, pp. 2883–2887, Dec. 2020.

[24] Q. Liu, D. Zhang, M. Tang, H. Deng, and D. Zhou, "A class of box-like bandpass filters with wide stopband based on new dual-mode rectangular SIW cavities," *IEEE Trans. Microw. Theory Techn.*, vol. 69, no. 1, pp. 101–110, Jan. 2021.

[25] Y. Zhu and Y. Dong, "A novel compact wide-stopband filter with hybrid structure by combining SIW and microstrip technologies," *IEEE Microw. Wireless Compon. Lett.*, vol. 31, no. 7, pp. 841–844, Jul. 2021.

[26] H.-Y. Xie, B. Wu, L. Xia, J.-Z. Chen, and T. Su, "Miniaturized half-mode fan-shaped SIW filter with extensible order and wide stopband," *IEEE Microw. Wireless Compon. Lett.*, vol. 30, no. 8, pp. 749–752, Aug. 2020.

[27] J. S. Hong and M. J. Lancaster, *Microstrip Filters for RF/Microwave Applications*. New York, NY, USA: Wiley, 2001.

RUSAN KUMAR BARIK (Member, IEEE) received the B.Tech. degree in electronics and communication engineering from the Biju Patnaik University of Technology, Rourkela, India, in 2012, and the M.Tech. degree in communication systems design and the Ph.D. degree in electronics engineering from the Indian Institute of Information Technology, India, in 2015 and 2018, respectively. He joined the Department of Electronics and Communication Engineering, Christ University, Bangalore, India, as an Assistant Professor, in 2018. In 2019, he joined as a Postdoctoral Researcher with the Department of Electrical and Electronic Engineering, Southern University of Science and Technology, Shenzhen, China. Currently, he is working as a Postdoctoral Researcher with the Engineering Optimization and Modeling Center (EOMC), Department of Electrical Engineering, Reykjavik University, Iceland. His research interests include multiband microwave devices, SIW components, surrogate-based modeling, and optimization.

SLAWOMIR KOZIEL (Fellow, IEEE) received the M.Sc. and Ph.D. degrees in electronic engineering from the Gdańsk University of Technology, Poland, in 1995 and 2000, respectively, and the M.Sc. degree in theoretical physics, the M.Sc. degree in mathematics, and the Ph.D. degree in mathematics from the University of Gdańsk, Poland, in 2000, 2002, and 2003, respectively. He is currently a Professor with the Department of Engineering, Reykjavik University, Iceland. His research interests include CAD and modeling of microwave and antenna structures, simulation-driven design, surrogate-based optimization, space mapping, circuit theory, analog signal processing, and evolutionary computation and numerical analysis.

STANISLAW SZCZEPANSKI received the M.Sc. and Ph.D. degrees in electronic engineering from the Gdańsk University of Technology, Poland, in 1975 and 1986, respectively. In 1986, he was a Visiting Research Associate with the Institute National Polytechnique de Toulouse (INPT), Toulouse, France. From 1990 to 1991, he was with the Department of Electrical Engineering, Portland State University, Portland, OR, on a Kosciuszko Foundation Fellowship. From August to September 1998, he was a Visiting Professor with the Faculty of Engineering and Information Sciences, University of Hertfordshire, Hatfield, U.K. He is currently a Professor with the Department of Microelectronic Systems, Faculty of Electronics, Telecommunications and Informatics, Gdańsk University of Technology. He has published more than 160 papers and holds three patents. His teaching and research interests include circuit theory, fully integrated analog filters, high-frequency transconductance amplifiers, analog integrated circuit design, and analog signal processing.